Solid State Phenomena Vol. 159 (2010) pp 27-38
© (2010) Trans Tech Publications, Switzerland
doi:10.4028/www.scientific.net/SSP.159.27

AlGaN/GaN based heterostructures for MEMS and NEMS applications

V. Cimalla[1], C.-C. Röhlig[1], V. Lebedev[1], O. Ambacher[1], K. Tonisch[2], F. Niebelschütz[2], K. Brückner[2], and M. Hein[2]

[1)]Fraunhofer Institute of Applied Solid State Physics, Tullastraße 72, 79108 Freiburg, Germany

[2)]Institute of Micro- and Nanotechnologies, Technical University Ilmenau, 98693 Ilmenau, Germany

volker.cimalla@iaf.fraunhofer.de

Keywords: Group III Nitrides, Microelectromechanical systems, piezoelectric actuation, resonator,

Abstract. With the increasing requirements for microelectromechanical systems (MEMS) regarding stability, miniaturization and integration, novel materials such as wide band gap semiconductors are receiving more attention. The outstanding properties of group III-nitrides offer many more possibilities for the implementation of new functionalities and a variety of technologies are available to realize group III-nitride based MEMS. In this work we demonstrate the application of these techniques for the fabrication of full-nitride MEMS. It includes a novel actuation and sensing principle based on the piezoelectric effect and employing a two-dimensional electron gas confined in AlGaN/GaN heterostructures as integrated back electrode. Furthermore, the actuation of flexural and longitudinal vibration modes in resonator bridges are demonstrated as well as their sensing properties.

Introduction to MEMS

Over the past decade microelectromechanical systems (MEMS) technology has evolved from a niche technology into an important mainstream technology for a wide range of applications [1-3]. Generally, MEMS are integrated systems,

- which combine electrical and mechanical components in order to
- sense its environment (mechanical sensors)
- have the ability to react to changes in that environment (actuators), and to
- analyze the data (electronics),
- which are fabricated by technologies for microelectronic devices, and
- which have a size in the order of micro- to millimeter.

Thus, MEMS are able to „feel", „think" and „react". A general block diagram for MEMS is given in Fig. 1.

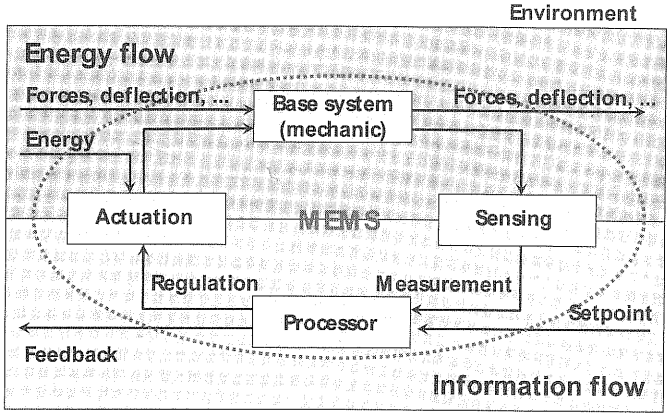

Fig. 1. Block diagram for the basic components in MEMS and their interaction.

The integrated micro-components make the system faster, more reliable, cheaper and capable of incorporating more complex functions [4]. Applications of such systems are manifold, including chemical, biological, and gas sensors, micro fluidic sensors and other fluid devices, micro-total analysis systems (μTAS), microactuators, rf MEMS up to high frequencies (filters, resonators, switches), micro-opto-electromechanical systems (MOEMS), and many others. The Si bulk and surface micromachining techniques have clearly led the way to MEMS commercialization. The first commercialized, less-integrated devices have been accelerometers, inkjet printer heads, and micromirrors for projection [5]. Further development was mainly driven by the automotive industry, which uses a variety of MEMS based sensors (e.g. acceleration, pressure, flow sensors [6]). The main advantage of a fully Si based technology is the possible integration to the existing technologies of electronic devices, such as CMOS.

Group III-nitrides for MEMS

The application of Si has shown limitations for sensing in harsh or at environmental conditions, a matter which has received increasing attention over the last years. Si cannot be used for high temperature applications since it looses the mechanical reliability at 500°C, it is attacked by corrosive media, and exhibits low biocompatibility, which restricts the usability in biosensing. As a consequence, sensing and actuating components have to be protected especially for chemical and for nanoscale sensors. As a consequence, such sensor are usually not integrated systems anymore. However, if single components are removed from the integrated system (see block diagram in Fig. 1) and have to be provided by periphery, they cannot be miniaturized and need to be calibrated with respect to periphery. For these reasons, they enable only very limited applications as small sensors. These drawbacks of the silicon based MEMS technology stimulated the search for more resistant materials such as wide band gap semiconductors.

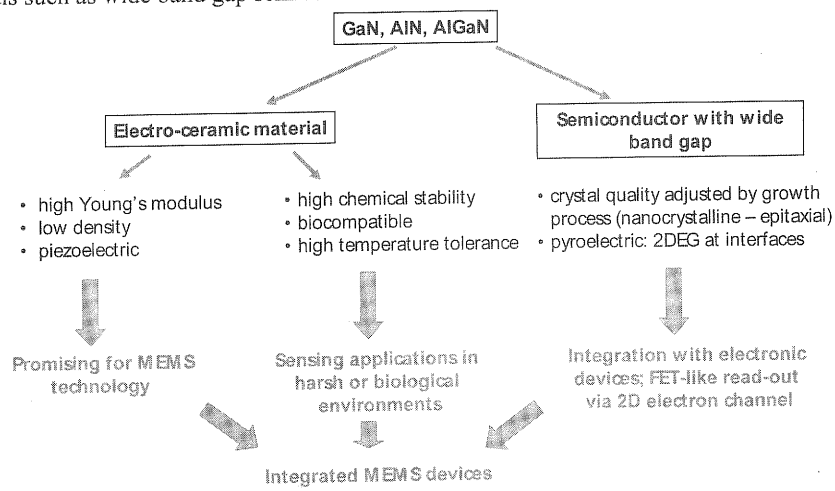

Fig. 2. Advantages of group III-nitrides for the realization of integrated MESM devices.

The group III-nitrides are potential representatives of wide band gap semiconductors for MEMS since they exhibit promising mechanical, electronic and sensing properties (see Fig. 2). They can be made insulating, semiconducting, conducting and piezoelectric depending on the doping and the design of heterostructures. These possibilities enable the fabrication of functional multilayers with fewer defects, which improves the operation of nanoscale devices and reduces the risks of corrosion. The high Young's modulus enables to achieve higher frequencies and quality factors in resonant devices at the same geometrical dimensions in comparison to Si [7]. Moreover, materials with a high Young's modulus can better maintain a linear relationship between applied load and the

induced deformation. Another major advantage is the very high mechanical, thermal, chemical, and biochemical stability [8,9]. They show no or very low reaction with molecules from the air, thus, these materials are very suitable for MEMS or NEMS, where the surface and small mass loads become more important. This is a precondition for reliable operation in environmental sensors. Finally, for group III-nitrides, electronic high frequency devices are well developed, which can be combined or integrated into the MEMS as amplifiers for rf devices. The pyroelectricity [10,11] offers completely new possibilities to integrate additional functionality into MEMS devices. AlGaN/GaN-heterostructures contain a highly conductive two-dimensional electron gas (2DEG) at the interface, which is sensitive to mechanical load, as well as to chemical modification of the surface, and can be used for novel sensing principles [12-14]. This 2DEG is influenced by several intrinsic and extrinsic properties and can be altered by (i) changes of the charges on the free, unpassivated gate surface, (ii) mechanical impact modulating the internal piezoelectric field, and (iii) directly by external fields, i.e. magnetic fields or electromagnetic radiation. This suggests that GaN based HEMTs are promising structures to sense those properties through modulation of the carrier density of the 2DEG. Passive microelectromechanical sensing devices employing the modulation of a 2DEG have been demonstrated previously such as membranes [15,16] and cantilevers [17,18]. However, the 2DEG can effectively used for integrated actuation as well [19].

Piezoelectric actuation

Group III nitrides are piezoelectric materials which provides further possibilities to integrate actuation principles. Piezoelectric actuation is based on the inverse piezoelectric effect [20]. The basic structure of a piezoelectrically driven MEMS resonator consists of a layer with a high Young's modulus combined with a low density film, providing the mechanical support, and an upper piezoelectric layer, which has to be 'clamped' by two (metallic) electrodes for applying the actuation voltage (Fig. 3) [21]. Conventional piezoelectric materials require thin film technologies, which are either hard to integrate, such as the sol-gel-process or screen-printing of lead zirconate titanate ceramics, or difficult to fabricate like the oriented crystal growth on metal surfaces in case of sputtered ZnO or AlN. Also the grain structure of such materials hinders the down-scaling of the devices and degrades the chemical stability. Although some material properties of the functional ceramics are superior in comparison to III-nitride semiconductors, the high structural quality and the dimensional control down to the monolayer level by epitaxial growth favor the application of semiconductors for nanoscale devices. Less defects and thus lower internal losses improve the operation behavior. The AlN-on-SiC cantilever [22] is an example for such a heterostructure. A major drawback, however, is the complex fabrication technology, in particular the realization of the back electrode in small MEMS and NEMS. Nanocrystalline AlN is a promising piezoelectric layer, which can be deposited on various substrates [23]. However, for integrated devices based on a heteroepitaxial system, new concepts have to be evaluated such as the use of doped passive layers or a

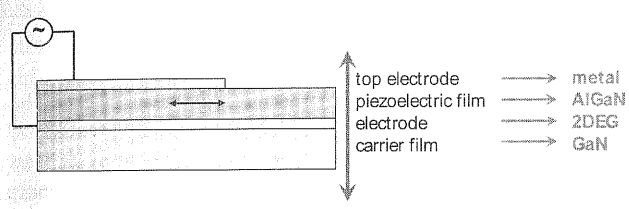

Fig. 3. Scheme of a piezoelectric driven cantilever and the replacements in the case of AlGaN/GaN heterostructures.

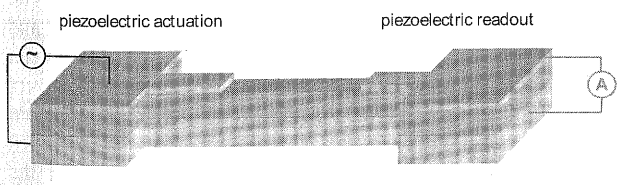

Fig. 4. Scheme of an integrated piezoelectric driven and sensed microelectromechanical bridge.

confined 2DEG as back electrode. In such epitaxial 'all-nitride' devices, an AlGaN/GaN heterostructure acts as the passive elastic component of the beam (Fig. 3). The 2DEG at the interface effectively acts as the back electrode and the thick, highly insulating AlGaN on top of it as the piezoelectric component.

Finally, a doubly clamped beam can by employed to realize a sensing scheme (Fig. 4), where one piezoelement actuates the beam, while a second piezoelement on the opposite side detects the displacement [24,25]. This concept has a high potential for the integration of small resonant devices. For thin films, the operation was demonstrated for ZnO/SiO_2 [26], and recently in an altered paddle configuration also for AlN/Pt/AlN [27].

Fabrication technology

For MEMS applications, free standing structures are usually prepared by isotropic undercutting of the active element. To realize suspended wide band gap semiconductor microstructures, principally the same micromachining techniques can be employed as for the highly developed Si technology [2,3,28]. They can be classified into bulk and surface micromachining (Fig. 5), which are based on a modified CMOS technology.

The bulk machining is based on the material removal from the bulk substrates. It can be performed by deep etching from the rear side, where the highly resistant functional group III-nitride layers on the front side acts as an etch stop, or by undercutting of a patterned functional layer from the front side. A major precondition for the realization of commercial wide band gap semiconductor based devices is the availability of large area substrates for the deposition of the functional layers. For the bulk micromachining of wide band gap semiconductors practically only Si and SiC substrates are available; for sapphire no selective etching techniques are known. Here, only surface micromachining can be used. In this case, microstructures are created by adding materials layer by layer on top of a substrate and the removal of at least one sacrificial layer by an etching technique, which is selective to the functional layers. All the three substrates have been used to produce free-standing AlGaN/GaN heterostructures with a confined 2DEG at the interface.

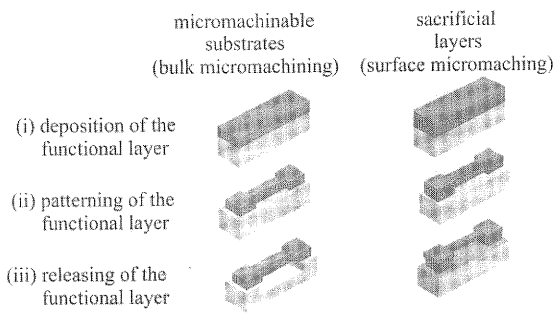

Fig. 5. Strategies for the fabrication of free-standing functional layers for MEMS applications.

For the deposition of the group III-nitrides, metal-organic chemical vapor deposition (MOCVD) with a commercial AIX200RF reactor (Aixtron) has been used, which is known to result in high-quality heterostructures on all the used substrates. Triethylgallium, trimethylaluminum and ammonia served as precursors with a V-III ratio of about 2000. The growth of the buffer and the AlGaN barrier layers was carried out at a temperature of 1120°C and a pressure of 15 mbar. The AlGaN barrier has a thickness about 30 nm and an Al content about 30%. Nucleation and intermediate layers were chosen in dependence on the substrate. More details about the growth can be found elsewhere for sapphire [29,31], SiC [31], silicon [19] and silicon with thin SiC interlayers [32]. On the sapphire substrates, nanocrystalline AlN layers with a thickness of 500 nm were grown as sacrificial layer prior to the MOCVD of AlGaN/GaN [29]

A summary of the used technologies as well as the advantages and disadvantages for the application of the most common substrates for wide band gap semiconductor based MEMS is given in table 1.

Table 1. Substrates for wide band gap semiconductor based MEMS.

on sapphire	on SiC	on silicon (/ SiC)
advantages		
+ stable up to high temperature + optically transparent + packaging (alumina and AlN ceramics [R95] are common housing materials)	+ bulk micromachining available + stable up to high temperature + good thermal conductivity	+ bulk micromachining available + well developed Si technology + potential integration to Si devices (CMOS)
disadvantages		
- no bulk micromachining	- expensive	- high defect density at the heterointerface, which degrade functional layers in NEMS - limited in operation temperature
fabrication strategy		
surface micromachining 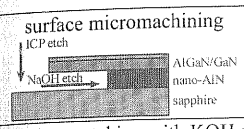	bulk micromachining 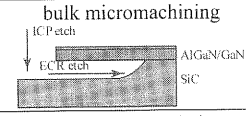	bulk micromachining 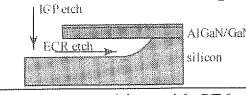
chemical wet etching with KOH and NaOH of sacrificial AlN layer	temperature assisted SF6 plasma etching of SiC substrate	ECR plasma etching with SF6 of Si substrate
realized resonator bridges		
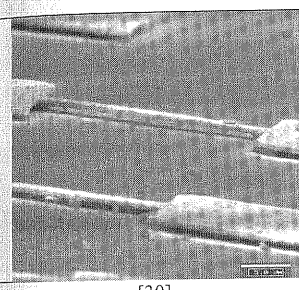	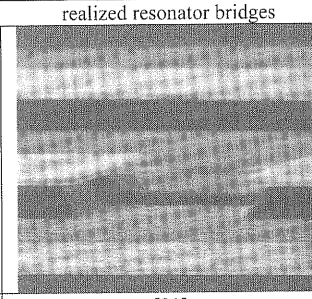	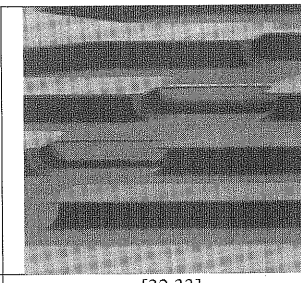
[30]	[31]	[32,33]

Optical lithography was used to define bridges with beam lengths l of 10 to 1000 μm and widths of 2 to 10 μm, respectively. An annealed and lift off patterned Ti/Al/Ti/Au layer system (20/80/30/100 nm) serves as back electrode for contacting the 2DEG and a Ti/Au layer system (10/50 nm) as top electrode [34]. Combinations of different anisotropic and isotropic etching processes were employed to realize the free-standing AlGaN/GaN microstructures. The whole MEMS process was developed to not affect the electrical properties of the integrated 2DEG [35]. The etching was performed by chlorine based inductive coupled plasma (ICP) etching of group III-nitrides [36], fluorine based electron cyclotron resonance (ECR) plasma etching of SiC [31] and silicon [33] as well as a NaOH based wet chemical etching of nanocrystalline AlN [30]. The resulting micromechanical structures (see table 2) were bridge-type resonators, which have shown to be sensitive to mass loading, pressure and temperature changes [37].

Piezoelectric actuation of the heterostructure

The processed heterostructures were further analyzed by piezoresponse force microscopy (Fig. 6 [38]). These measurements were performed using a modulation voltage of 10 kHz with and without a negative DC offset voltage.

The piezoelectric displacement is shown in Fig. 7 over a modulation voltage range from 0 to 5 V for different dc offsets ranging from 0 to 5 V. The measured piezoelectric response is strongly affected by applying a dc offset and reaches a saturation value for large modulation voltages. The highest piezoelectric modulus d_{33} was determined to be 4.1 pm/V and could only be found for small

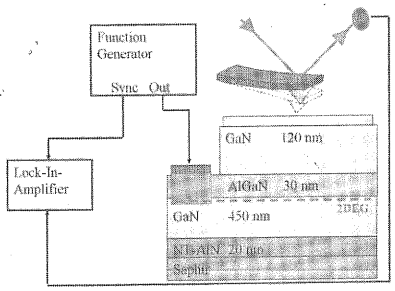

Fig. 6. PFM measurement setup with 2DEG as back contact and metal top electrode [34,38].

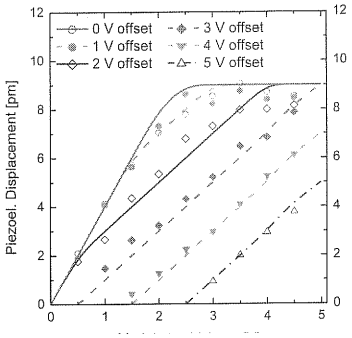

Fig. 7. Piezoelectric displacement from PFM measurements versus the applied modulation voltage amplitude [34].

modulation voltages and small to zero dc offsets. Obviously, a narrow operational voltage range of -4 V to approximately 1 V exists, where unaffected modulation can be used. For higher voltages, only parts of the actuation voltage contribute to the piezoelectric response. For large positive offsets of 3 to 5 V, the modulation with small amplitudes does not lead to any measurable piezoelectric response at all. In this case, the whole modulation takes place in the positive voltage range (diode like forward operation), where large current densities screen the electric field. Only when the modulation voltage becomes larger, the negative half wave of the modulation reaches an operation range with lower current densities (still in forward operation), thus resulting in a small piezoelectric displacement.

However, since only one half wave of the modulation causes piezoelectric response, the effective d_{33} is also only half of the original value, thus resulting in a lower slope of 2 pm/V (see Fig. 7). Only for zero dc offset, both half waves of the modulation contribute to the piezoelectric actuation resulting in a steeper slope with $d_{33} = 4.1$ pm/V.

Saturation of the piezoelectric response was finally reached for large modulation amplitudes, when the negative half cycle causes depletion of the 2DEG. Thus, saturation is reached when the piezoelectric response to the modulation voltage is limited on both sides: due to the depletion of the 2DEG (neg. voltage) and due to high current densities (pos. voltage) [34]. As a consequence, for effective piezoelectric actuation of AlGaN/GaN heterostructures employing the 2DEG as back electrode, the driving voltage has to be biased negatively and is limited to $\Delta V \sim 5 \ldots 6$ V (Fig. 8).

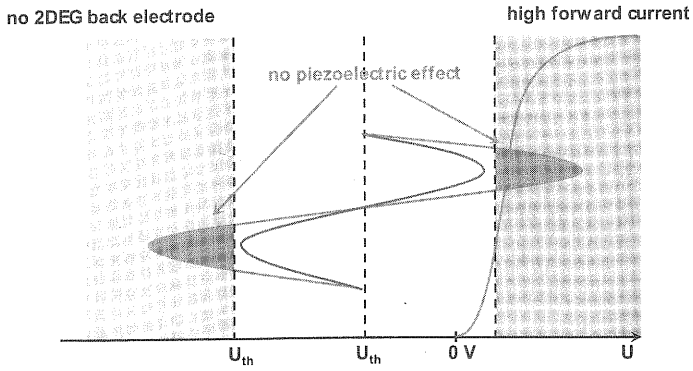

Fig. 8. Limitations for the piezoelectric actuation of AlGaN/GaM heterostructures employing the 2DEG as back electrode [32].

Piezoelectric actuation of resonator bars

Using the determined operation conditions, suspended AlGaN/GaN beams were actuated [19]. Caused by the piezoelectric modulus $d_{31} \approx 2$ pm/V, the horizontal elongation of the upper AlGaN layer and its offset from the neutral axis generate a bending moment that leads to an out-of-plane deflection. To achieve piezoelectric excitation of flexural oscillations of a selected resonator beam, frequency sweeps of monofrequent harmonic driving voltages with peak values V_D varying between 500 mV and 1.5 V were applied to the appropriate contact areas through coplanar contact probes. The time-dependent out-of-plane deflection was analyzed by a scanning laser-Doppler vibrometer (Polytec MSA-400), which offers dynamic characterization up to 10 MHz with a sufficient spatial resolution in lateral (< 1 µm) and vertical (< 0.1 pm/Hz$^{1/2}$) dimension. The maximum deflection amplitudes u_{max} and typical mode shapes from scanning along the length of a 500 µm long beam are shown in Fig. 9 (top) for the fundamental mode and its 8th harmonic. Although the electromechanical coupling coefficients η_n decrease for increasing mode numbers n due to a progressing mismatch of the vibration sections to the lengths of the top electrodes, all resonant frequencies f_n of each probed resonator were detected up to the frequency limit of the vibrometry measurement system. The resonant peaks for the flexural out-of-plane vibration modes are shown in the spectra of Fig. 9 (bottom) for two resonator beams of different length. The measurement was performed under normal ambient conditions, resulting in Q-factors about 100 which were limited by viscous damping in air.

MEMS resonator chips with 5 µm and 10 µm wide doubly-clamped beams having lengths l between 80 and 1000 µm were further investigated systematically. The results for the lowest eight resonant modes ($1 \le n \le 8$) that exhibit resonant frequencies up to 8.1 MHz are compiled in Fig. 10 [19]. Double-logarithmic scaling was chosen to emphasize the power-law dependence $f_n \sim l^b$ of the resonant frequency on the beam length l.

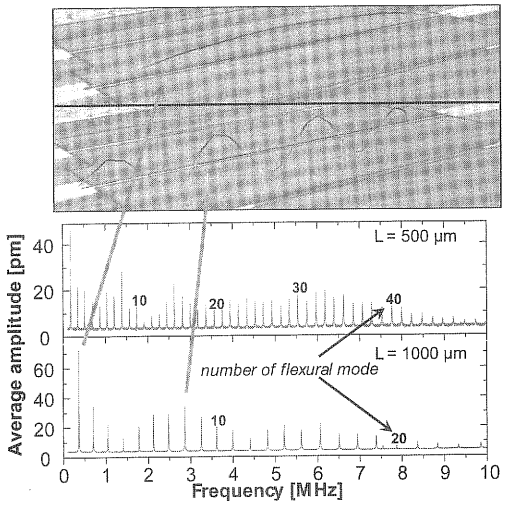

Fig. 9. Exemplary mode shapes of the first (top panel) and the 8th (second panel) out-of-plane flexural resonances of a 500 µm long and 5 µm wide AlGaN/GaN beam resonator under piezoelectric actuation (V_D = 0.5 V) monitored by laser-Doppler vibrometry. Bottom panels show the spectra of the average out-of-plane displacement for the two resonator beams [19].

For the fundamental flexural mode (n = 1), the resonant frequency f_1 can be expressed by [39]:

$$f_1 = 1.03\sqrt{\frac{E_{GaN}}{\rho_{GaN}}}\cdot\frac{t}{l^2}\cdot\sqrt{1+\gamma_1(\varepsilon)\frac{l^2}{t^2}\varepsilon} \quad (1)$$

Here, E_{GaN} denotes the Young's modulus of the dominating beam material GaN, ε the axial strain, and $0.22 \le \gamma_1(\varepsilon) \le 0.29$ a strain-dependent coefficient. According to Fig. 10, the slope of each $f(l)$-curve was found slightly below -1. In terms of Eq. (1) such a sub-linear dependence indicates a high residual strain within the AlGaN/GaN layer, yielding the highest possible f_n-values. The tensile strain was determined to be $\varepsilon = 2.8\times10^{-3}$.

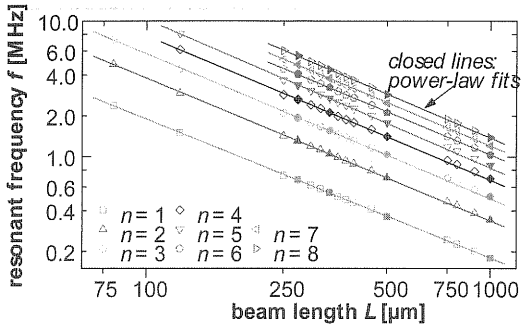

Fig. 10. Resonant frequency f_n of the n^{th} flexural vibration mode ($1 \le n \le 8$) versus beam length l on double-logarithmic scales. The measurement was carried out for a set of 5 µm (filled symbols) and 10 µm wide (open symbols) doubly-clamped beams with lengths l between 80 and 1000 µm. The lines represent power-law fits, yielding slopes slightly below -1 for all data sets [19].

Piezoelectric read-out of resonator bars

Using the coupled piezoelectric microstructure of Fig. 4, both piezoelectric actuation and sensing were performed with the same heterostructure [40]. The measurements inside of a vacuum wafer prober allow the variation of the ambient measuring conditions from 10^{-5} mbar to 10^{3} mbar. Fig. 11 shows the resonant frequencies up to the fourth longitudinal mode in dependence on the beam length, from $175 \le l \le 1000$ µm.

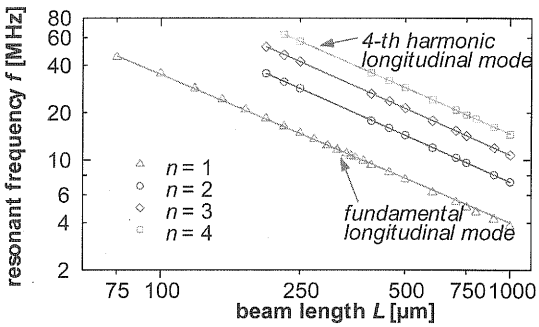

Fig. 11. Resonant frequency f_n of the nth longitudinal vibration mode in vacuum, for $1 \le n \le 4$, versus beam length l on double-logarithmic scales. Solid lines represent the linear fit of the slopes resulting in values of b close to 1. [40]

The observed resonant frequencies can be described Lamb waves (Fig. 12 [41]). These longitudinal vibration modes can be described by lateral standing bulk acoustic waves, which occur

at frequencies where integer multiples of the half wavelength coincide with the geometric dimensions of the resonator. Thus, the resonant frequencies f_n of the n^{th} harmonic resonant longitudinal mode are given by equation:

$$f_n = c_1 / \lambda = n \cdot c_1 / (2l), \quad (2)$$

where n is the mode number, c_1 the phase velocity, λ the wavelength and l the beam length [40]. The phase velocity c_1 depends on the excited wave mode and can be estimated as:

$$c_1 = \sqrt{E_{GaN} / \rho_{GaN}}, \quad (3)$$

with E_{GaN} as Young's modulus and ρ_{GaN} as mass density of the dominating beam material GaN. In case of very thin beams, i.e. a thickness t much smaller than the lateral acoustic wavelength λ, this phase velocity c_1 is representative for Lamb wave resonators [42] to which the doubly clamped AlGaN/GaN-resonators can be referred to. According to Fig. 11, the linear fit of the slopes resulting in values of b close to 1 following equ. (2) and for the phase velocity a value of c_1 = 7500 m/s was determined for the AlGaN/GaN-resonators, which is in very good agreement with results from literature obtained from measurements of AlGaN layers of a slightly lower tensile stress level [43].

Fig. 12. Longitudinal and flexural modes on bridge type resonators.

Sensing properties

Resonator bars similar to the structures investigated in this work have shown various sensing effects [24,35-40,44,45] including mass loading, pressure and temperature sensing. In this work, the influence of the ambient pressures on the quality factor of the integrated AlGaN/GaN-resonators was further analyzed [40]. Therefore, electrical response was measured around the fundamental resonant frequencies f_1 of 3.794 MHz and 7.536 MHz for the 1000 µm and the 500 µm long beam, respectively. The quality factors were determined by curve fitting assuming a Lorentzian frequency response superimposed by a frequency-independent background signal. For the resonators analyzed in Fig. 13, the Q factors were determined to decrease from 2800 in vacuum to 1250 at normal ambient conditions. The resonant vibration and with that the quality factor Q is unaffected at pressures below 5 mbar, where intrinsic losses and the molecular flow are the dominating damping effects, respectively. In the region above 5 mbar the damping mechanism of viscous flow decreases the quality factor with a comparable sensitivity.

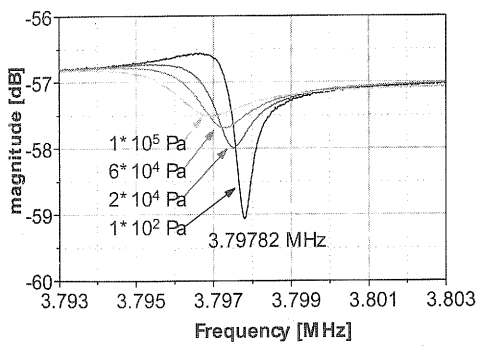

Fig. 13. Pressure dependence of the transmission coefficient of a 1000 µm long and 5 µm wide resonator bridge. Resonant frequency and quality factor decrease as the pressure is increased [19].

In addition to the curves shown in Fig. 13, the pressure dependence of the doubly-clamped longitudinal mode beam resonators is further analyzed for the fundamental mode of two resonators of lengths l = 500 and 1000 µm and, for the shorter beam, also for the 2nd harmonic mode. The second harmonic of the 500 µm long beam was found at f_2 = 14.425 MHz. For comparison, the $Q(p)$-curve of a 100 µm long doubly clamped flexural bending beam resonator (f_1 = 559 kHz) is included in the diagram [39].

The total Q-factor can be described as $Q^{-1}(p) = Q^{-1}_{vac} + Q^{-1}_{fluid}(p)$, where Q_{vac} and $Q_{fluid}(p)$ represent the intrinsic and the pressure dependent fluid damping losses, respectively. At pressures below about 5 Pa, the vibrations are unaffected by the environment and the Q-factor is dominated by intrinsic and clamping losses. In the region of molecular damping, a pronounced Q-drop can be observed for the flexural bending mode. In the continuum of viscous flow, for $p > 1$ kPa, the Q-factors of the longitudinal modes also decrease but with a lower sensitivity $\delta\log(Q)/\delta(\log(p))$ compared to the flexural mode beam in the molecular region. In the viscous region, $Q_{fluid} \sim p^{-1/2}$ for the flexural mode, which seems to hold for the longitudinal modes, too. This overall behavior is expected as the mechanical deflections of the acoustic modes are much smaller than those of the flexural bending modes. Similar results for $Q(p)$ have been obtained from measurements for contour-mode MEMS resonators [46,47]. The Q-factor for ambient conditions was found to be of the same order of magnitude as the vacuum value Q_{vac}. Hence, intrinsic Q_{vac} and external Q_{fluid} are of comparable magnitude. For the 2nd harmonic longitudinal mode of the 500 µm long beam, the intrinsic losses were found to exceed the viscous losses under ambient conditions leading to a reduced sensitivity of $Q(p)$ [40].

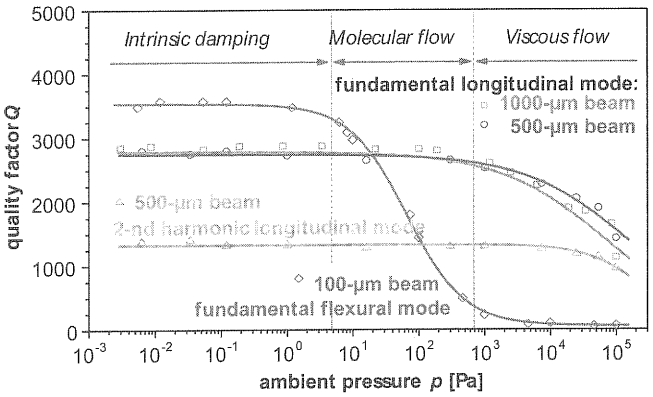

Fig 14. Comparison of the pressure dependence of the quality factor Q of the fundamental longitudinal and flexural vibration modes. The lines are fits according to the analytical models described in Ref. [40].

Despite the lower sensitivity on pressure, longitudinal mode resonators can be advantageous in sensor applications where the high Q is maintained in gaseous and presumably as well in liquid environments, which simplifies the detection in contrast to the low-Q flexural mode devices. Compared to the reported Q-factors of several hundred thousands for the flexible supported contour-mode devices, the values of the doubly clamped longitudinal mode MEMS resonators of this study are by far lower. It is tempting to speculate that the coupling of mechanical energy into the substrate at the clamping points is a possible source of losses, which has to be studied in more detail.

Summary

We have demonstrated fully integrated piezoelectric actuated and sensing doubly-clamped AlGaN/GaN MEMS resonators where an integrated 2DEG has been employed as back electrode. The vibration modes were consistently characterized by scanning laser-Doppler vibrometry and a piezoelectric sensing scheme has been demonstrated. The measured resonant frequencies between 0.2 and 63 MHz and their vibration amplitudes could be related to geometry and material parameters of the MEMS resonators. Facilitating all-electrical transduction, the electromechanical coupling was found to be much higher for the longitudinal modes than for the flexural bending

modes. The Q-factors of several thousands under vacuum decreased to values about one thousand under normal ambient pressure. The highest sensitivity was observed in the region of viscous damping which may be utilized in future sensor applications for the determination of the properties of gaseous or even liquid fluids. Improvements of the actuation and read-out schemes including the reduction of the background signal will be faced next.

Acknowledgement

This work has been funded by the German Research Foundation (DFG), Priority Program 1157 'Integrated electroceramic functional structures' (Grants HE3642/2 and AM105/2) and Priority Program 1165 'Nanowires and Nanotubes' (Grant CI148/2) as well as the Fraunhofer grant "Attract".

References

[1] Gardner J W 1994 Microsensors: Principles and application (Chichester, UK: Wiley)

[2] Hsu T-R 2002 MEMS and Microsystems: Design and Manufacture (New York: McGraw-Hill)

[3] Lyshevski S E 2005 Nano- and Micro-Electromechanical Systems: Fundamentals of Nano- and Microengineering (Boca Raton, Florida: CRC Press)

[4] Varadan V K 2003 Proc. SPIE 5062 20

[5] Korvink J G and Paul O (eds.) 2006 MEMS: a practical guide to design, analysis and applications (Norwich, NY: Springer)

[6] Flik G, Eisenschmid H, Raudzis C, Schatz F, Schoenenborn W and Trah H-P 2002 Mater. Res. Soc. Symp Proc 687 B1.1

[7] Ekinci K L and Roukes M L 2005 Rev. Sci. Instrum. 76 061101

[8] Jackson K M, Edwards R L, Dirras G F and Sharpe Jr. W N 2002 Mater. Res. Soc. Symp. Proc. 687 B6.3

[9] Edgar J H, Strite S, Akasaki I, Amano H, and Wetzel C (eds.) 1999 Processing and Applications of Gallium Nitride and Related Semiconductors (E M I S Datareviews Series) (Institution of Electrical Engineers) London, UK

[10] Ambacher O 1998 J. Phys. D: Appl. Phys. 31 2653

[11] Ambacher O et al.2002 J. Phys.: Condens. Matter. 14 3399

[12] Eickhoff M et al 2003 Phys. Status Solidi (c) 0 1908

[13] Stutzmann M, Steinhoff G, Eickhoff M, Ambacher O, Nebel C E, Schalwig J, Neuberger R and Müller G 2002 Diam. Relat. Mater. 11 886

[14] Pearton S J, Kang B S, Kim S, Ren F, Gila B P, Abernathy C R, Lin J and Chu S N G 2004 J. Phys.: Condens. Mater. 16 R961

[15] Eickhoff M, Ambacher O, Krötz G and Stutzmann M 2001 J. Appl. Phys. 90 3383

[16] Kang B S et al. J 2005 Appl. Phys. Lett. 86 253502

[17] Kang B S et al. 2003 Appl. Phys. Lett. 83 4845

[18] Zimmermann T, Neuburger M, Benkart P, Hernández-Guillén F J, Pietzka C, Kunze M, Daumiller I, Dadgar A, Krost A and Kohn E 2006 IEEE Electron Device Lett. 27 309

[19] Brueckner K, Niebelschuetz F, Tonisch K, Michael S, Dadgar A, Krost A, Cimalla V, Ambacher O, Stephan R, and Hein M A, 2008 Appl. Phys. Lett. 93 173504.

[20] Zelenka J 1986 Piezoelectric Resonators and their applications (Amsterdam, Oxford, New York, Tokyo: Elsevier)

[21] DeVoe D L and Pisano A P 1997 J. Microelectromech. Syst. 6 266

[22] Doppalapudi D, Mlcak R, Chan J, Tuller H L, Abell J, Li W and Moustakas T D 2004 Electrochem. Soc. Proc. 2004-06 287

[24] Cimalla V, Pezoldt P, and Ambacher O, 2007 J. Phys. D: Appl. Phys. 40 6386.

[25] DeVoe D L 2001 Sens. Actuators A 88 236

[26] Kouh T, Karabacak D, Kim D H and Ekinci K L 2005 Appl. Phys. Lett. 86 013106

[27] Piazza G and Pisano A P 2007 Sens. Actuators A, doi:10.1016/j.sna.2006.12.003

[28] Elwenspoek M and Jansen H V 2004 Silicon Micromachining (Cambridge, UK: Cambridge University Press)

[29] Tonisch K, Cimalla V, Niebelschütz F, Romanus H, Eickhoff M, and Ambacher O, 2007 phys. stat. sol. (c) 7 2248.

[30] Tonisch K, Niebelschuetz F, Cimalla V, Romanus H, and Ambacher O, 2007 MRS Symp. Proc. 955 I16-03.

[31] Stauden Th, Niebelschütz F, Tonisch K, Cimalla V, Ecke G, Haupt Ch, and Pezoldt J, 2008 Mater. Sci. Forum 600-603 651.

[32] Tonisch K: Thesis, Technical University Ilmenau, 2009.

[33] Förster Ch, Cimalla V, Brueckner K, Lebedev V, Stephan R, Hein M and Ambacher O 2005 Phys. Status Solidi (a) 202 671

[34] Tonisch K, Buchheim C, Niebelschütz F, Schober A, Gobsch G, Goldhahn R, Cimalla V, and Ambacher O., 2008 J. Appl. Phys. 104 084516

[35] Niebelschütz F, Cimalla V, Tonisch K, Haupt Ch, Brückner K, Stephan H, Hein M E, and Ambacher O, 2008 phys. stat. sol. (c) 5 1914

[36] Niebelschütz F, Cimalla V, Brückner K, Stephan H, Tonisch K, Hein M A, and Ambacher O, 2008 Proc. IMechE Vol. 221 Part N: J. Nanoengineering and Nanosystems, 221 (N2) 59

[37] Cimalla V, Niebelschütz F, Tonisch K, Foerster Ch, Brückner K, Cimalla I, Friedrich T, Pezoldt J, Stephan H, Hein M E, and Ambacher O, 2007 Sens. Actuat. B 126 24.

[38] Tonisch K, Cimalla V, Foerster Ch, Romanus H, Ambacher O, and Dontsov D, 2006 Sens. Actuat. A 132 658.

[39] K. Brueckner, Cimalla V, Niebelschütz F, Stephan H, Tonisch K, Ambacher O, Hein M A. 2007 J. Micromech. Microeng. 17 2016.

[40] K. Brueckner et al., 2009 Proc. of the 22nd IEEE International Conference on Micro Electro Mechanical Systems, Sorrento, Italy, 2009, pp. 927.

[41] Ballantine D S, White R M, Martin S J, Ricco A J, Zellers E T, Frye G C, and Wohltjen H, Acoustic wave sensors, (Academic Press, 1st edn., San Diego, 1997), p. 115.

[42] Bjurström J, Katardjiev I, and Yantchev V, 2005 Appl. Phys. Lett. 104 154103.

[43] Jiménez Riobóo R J, Rodríguez-Cañas E, Vila M, Prieto C, Calle F, Palacios T, Sánchez M A, Omnès O, Ambacher O, Assouar B, and Elmazria O, 2002 J. Appl. Phys. 92 6868.

[44] Brückner K, Cimalla V, Niebelschütz F, Stephan H, Tonisch K, Ambacher O, and Hein M A, 2007 6th IEEE Conference on Sensors October 28 - 31, 2007, Hyatt Regency Atlanta, Atlanta, Georgia, USA, 2007, p. 1251.

[45] Tonisch K, F. Will, Förster Ch, V.Cimalla, K. Brueckner, Hein M E, and Ambacher O, 2005 7. Dresdner Sensor-Symposium, Dresden, 12.-14. 12. 2005, Dresden, TUD Press, Dresden p. 239.

[46] Wang J, Ren Z, and Nguyen C-T C, 2004 IEEE Trans. Ultrason. Ferroelectr. Freq. Control, 51, 1607.

[47] Lee J-E Y, Zhu Y, and Seshia A A, 2008 J. Micromech. Microeng., 18 064001.